THE INTELLIGENT COMPUTING AND INFORMATION TECHNOLOGY IN SPORTS PERFORMANCE EVALUATION

YUANYUAN ZHANG,* HUAN LONG,† AND LEI JING‡

Abstract. This paper presents a new method to obtain the training trajectory by using the mean shift method. In this way, the incomplete motion trajectory caused by the rapid movement of the moving target due to the complex background is solved. The human body modeling is regarded as a skeletal model with 51 degrees of freedom and 16 joints, and the motion trajectory is digitally processed. At the same time, the dimension compression of the trajectory is also carried out to reduce the calculation amount. The gradient iteration method based on random distribution is selected to reduce the dependence on environmental parameters. The object color image is the main feature to realize the acquisition of motion trajectory. The experiment proves that the algorithm can reflect the movement state of each part of the athlete well. This method can accurately obtain the training trajectory without any associated parameters.

Key words: Digital learning; Data dimensionality reduction; Average shift algorithm; Gradient iteration method

1. Introduction. MPEG is the expert group on moving images [1]. The algorithm has the advantages of less redundancy and better overall stability, while H.263 algorithm has higher efficiency. In addition, in order to ensure the complete coding of the tested object, the tested object must be separated during video compression [2]. However, the existing compression methods cannot effectively retrieve the video, so there are some difficulties in the effective segmentation of the image. MPEG-4, introduced in 2000, added the ability to retrieve multiple semantic objects based on context and foreground [3]. It can effectively improve the compression efficiency. However, it has poor denoising ability during compression [4]. But a lot of experiments prove that these algorithms cannot accurately describe the pose of the subject and the segmentation effect is not obvious. In this project, the fuzzy clustering method is used to deeply study the motion attitude of the target object, so as to realize the effective use and analysis of the motion video.

2. Motion video fuzzy clustering image segmentation. In order to solve the problems of random posture, unclear change law and difficult to judge the range of motion video, a method of motion video detection and segmentation is proposed. It can distinguish the moving position area and the invalid pixel in the image into the front and back parts. In the process of motion video recording, the method based on fuzzy clustering is used to segment motion video recording [5]. The motion of the object is predicted and compensated by image analysis. Construct multiple images with small intervals into the same background [6]. Then, the boundary extraction technique is used to segment the object's boundary to obtain the background image. Eliminate the foreground area to get the background area. The block diagram of image segmentation is shown in Figure 2.1.

When selecting fuzzy objects, people must first consider what features can accurately depict the moving posture; The second is that the motion posture in the image and the image between the invalid image cannot be completely consistent, and there should be a big difference between the two. After the motion is predicted and compensated, the moving objects in the moving video can be represented by small spaced backgrounds with similar backgrounds [7]. The feature of grayscale can be used when selecting the fuzzy feature. In addition, in view of the problem that a single fuzzy feature is not conducive to segmentation results, this project intends to transform the division of moving position region and invalid pixel region into the processing of non-normal feature distribution pixels [8].

---
*North China Institute of Science and Technology, Langfang 065201, China (Corresponding author, zyyncist2024@163.com)
†North China Institute of Science and Technology, Langfang 065201, China
‡North China Institute of Science and Technology, Langfang 065201, China
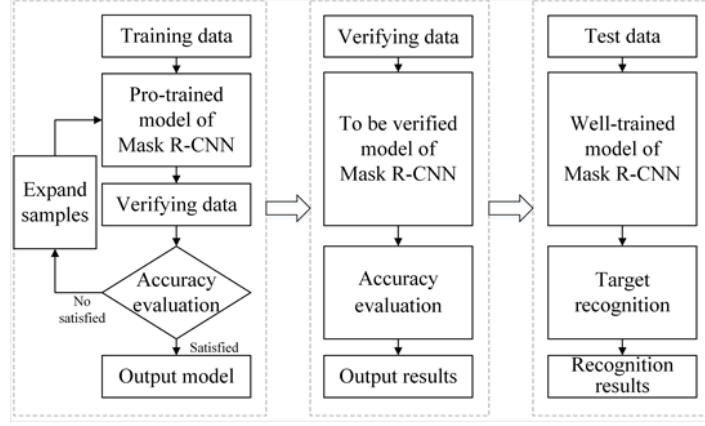
Fig. 2.1: Block diagram of sports image segmentation.

3. Use Mean Shift algorithm to train tracking data capture. Aiming at the fast moving and complex background of objects captured in sports, an average displacement method is proposed to track the trajectory of objects. Measurement is a non-parametric kernel density estimation method based on gradient iteration [9]. It is independent of the associated parameters and has a high convergence rate. The following illustrates the core density estimation of the algorithm: point u in the set is as follows:

$$\hat{g}(u) = \frac{1}{nl^d} \sum_{i=1}^{n} H\left(\frac{u - U_i}{l}\right) \tag{3.1}$$

l represents the window radius, H represents the kernel function, and then the Epanechnikov kernel is used to minimize the mean deviation between the estimated and the true density. Its formula is:

$$H_{P(u)} = \begin{cases} \frac{1}{2}z_d^{-1}(d+2)\left(1 - \|u\|^2\right) & \text{if } \|u\| < 1 \\ 0 & \text{else} \end{cases} \tag{3.2}$$

z_d is the volume of the ball. In general, H is a function of $\|u\|^2$, and $H(u) = h\left(\|u\|^2\right), h : [0, \infty) \to S$ is a shape function of the H kernel. Epanechnikov's shape function can be expressed as:

$$H_{P(u)} = \begin{cases} \frac{1}{2}z_d^{-1}(d+2)(1-u) & \text{if } u < 1 \\ 0 & \text{else} \end{cases} \tag{3.3}$$

From the above formula, it can be seen that h represents inconstant, nonnegative, piecewise continuity, and conforms to $\int_0^\infty h(u)du < \infty$. By replacing the distribution function of formula (3.2) in formula (3.3), we get:

$$\hat{g}_{H(u)} = \frac{1}{nl^d} \sum_{i=1}^{n} H\left(\left\|\frac{u - U_i}{l}\right\|^2\right) \tag{3.4}$$

l^d stands for ball height. If the core function $h(u)$ is derivable in the range $u \in [0, \infty)$, then it is assumed to be $y(u) = -h'(u)$, and at this time $y(u)$ is considered to be typical of the core function, and this core function can also be expressed as $Y(u) = Zy\left(\|u\|^2\right)$, where Z is a normalized constant, if the estimated gradient value is used as the baseline, the estimated probability density gradient can be obtained:

$$\hat{\nabla}_u g_{H(u)} \nabla_u \hat{g}_{H(u)} = \frac{1}{nl^d} \sum_{i=1}^{n} \nabla_u H\left(\frac{u - U_i}{l}\right) \tag{3.5}$$

For $u_1, u_2, \ldots, u_n, \nabla_u$ is a gradient factor. The offset mean vector of the core function Y can be obtained as follows:

$$M_{l,Y}(U) = \left[\frac{\sum_{i=1}^{n} u_i y \left(\left\| \frac{u - U_i}{l} \right\|^2 \right)}{\sum_{i=1}^{n} y \left(\left\| \frac{u - U_i}{l} \right\|^2 \right)} - u \right] \tag{3.6}$$

The density estimates of u can be obtained from Y:

$$\hat{g}_{Y(u)} = \frac{Z}{nl^d} \sum_{i=1}^{n} H \left(\left\| \frac{u - U_i}{l} \right\|^2 \right) \tag{3.7}$$

M is a constant, and (3.4) can be reduced to:

$$\hat{\nabla}_u g_{H(u)} = \hat{g}_{Y(u)} \frac{2/Z}{l^2} M_{l,Y(u)} \tag{3.8}$$

It follows that:

$$M_{hY(u)} = \frac{l^2}{2/Z} \times \frac{\hat{\nabla}_u g_{H(u)}}{\hat{g}Y(u)} \tag{3.9}$$

From formula (3.8), it can be seen that the average-displacement vector obtained from Y coincides with the concentration gradient obtained from H. Therefore, a series of changes at the center point of the core function is taken as $y_j, j = 1, 2, \ldots,$, and then:

$$y_{j+1} = \frac{\sum_{i=1}^{n} u_i y \left(\left\| \frac{y_j - u_i}{l} \right\|^2 \right)}{\sum_{i=1}^{n} y \left(\left\| \frac{y_j - u_i}{l} \right\|^2 \right)} \tag{3.10}$$

y_{i+1} is the weighted average of y_j points calculated using the value of the kernel function, and y_1 is the original positioning [10]. Then the motion characteristics extracted by the average method are used to collect the motion trajectory. The color information remains unchanged when the object is translated, rotated, or deformed. This is one of the most believable image features.

Suppose $U = \{u_1, \ldots, u_N\}$ contains N sampling points and $p(u) = N(u, \delta, N)$ represents the probability distribution, where δ represents the mean vector and Q represents the covariance matrix. If the training object is elliptical, the selected object in this frame is initialized first. u_i is used to represent the specific position of the pixel owned by the entire player, δ_0 is the starting point, and T is the move cycle [11]. The general shape of this goal can then be expressed as:

$$Q_0 = \sum (u_i - \delta_0)(u_i - \delta_0)^T \tag{3.11}$$

An image segmentation method based on color histogram is proposed, which divides the color image into M subregion and uses $b(u_i) : S^2 \to 1, \ldots, M$ function to determine the color degree of each region u_i of the image [12]. The m subinterval is resolved as follows:

$$w_m = \sum_{i=1}^{N_{Q_0}} N(u_i; \delta; Q_0) \varphi[b(u_i) - m] \tag{3.12}$$

Where φ represents the Kronecker function and N represents the Gaussian kernel, the central part of the object is weighted to the maximum, and then N_{Q0} pixels close to the core are used as sub-intervals. Elements other than 2.5σ are not considered during processing to reduce the operational burden [13]. If the object to be

Table 4.1: Statistics of SA values.

Segmentation method	Tier 1	Tier 2
Fuzzy clustering algorithm	0.0776	0.2200
MPEG-4	0.1285	0.2993
Frequency domain segmentation	0.1384	0.4414
Time domain segmentation	0.2728	0.3463

captured appears in an image, then the capture finds the captured object in a new image, and then determines the position of the object in the new sequence by calculating the similarity between the real object and the object to be captured. In this way, the color rendering $s(\delta, Q)$ of the captured object can be determined by the color histogram, then the following values of m color parts can be obtained:

$$s_m(\delta, Q) = \sum_{i=1}^{N_v} N(u_i; \delta; Q) \varphi[b(u_i) - m] \tag{3.13}$$

The Bhattacharyya coefficient is used to judge the following approximation of the two-color subspaces:

$$\zeta[s(\delta, Q), w] = \sum_{m=1}^{M} \sqrt{s_m(\delta, Q)} \sqrt{w_m} \tag{3.14}$$

A Taylor extension of the estimate $s(\delta^{(h)}, Q^{(h)})$ is as follows:

$$\zeta[s(\delta, Q), w] \approx z_1 + z_2 \sum_{m=1}^{N_s} \mu_1 N(u_i; \delta, Q) \tag{3.15}$$

z_1, z_2 is the Lagrange daily number and μ_i is the Bhattacharyya coefficient, which is calculated as follows:

$$\mu_i = \sum_{m=1}^{M} \sqrt{\frac{w_m}{s_m(\delta^{(h)}, Q^{(h)})}} \varphi[b(u_i) - m] \tag{3.16}$$

In order to achieve the closest similarity between the captured tracking data and the real object, the maximum value in the formula (3.16) must be used.

4. Experimental results and analysis.

4.1. Spatial accuracy. This project takes the 2022 UCLA game video as the research object. Two continuously transformed moving images were selected for morphological filtering and correction respectively [14]. The spatial accuracy of each image was evaluated using the following formula:

$$SA = \frac{\sum_{(u,v)} \phi^{ext}(u, v) \oplus \phi^{ref}(u, v)}{\sum_{(u,v)} \phi^{ref}(u, v)} \tag{4.1}$$

(u, v) represents the pixel, ϕ^{ext} represents the partition range of the image; ϕ^{ref} is the partition of the completed moving object; The operation symbol $\oplus$ represents the additivity of logic. Generally speaking, the segmentation of images with fewer logarithms has higher spatial accuracy [15]. The SA values obtained by various algorithms are shown in Table 4.1. The results show that the proposed fuzzy clustering algorithm has the least SA. It can fill the blank of sports video efficiently. It can accurately segment images with large effects such as background and color. It has high spatial and temporal accuracy.
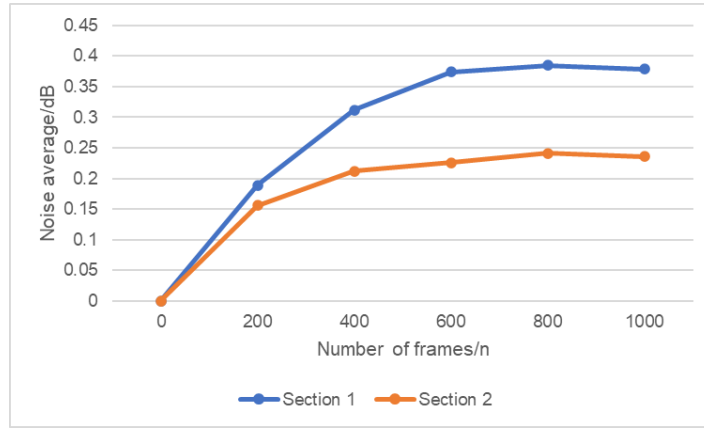
Fig. 4.1: Average image noise curve.
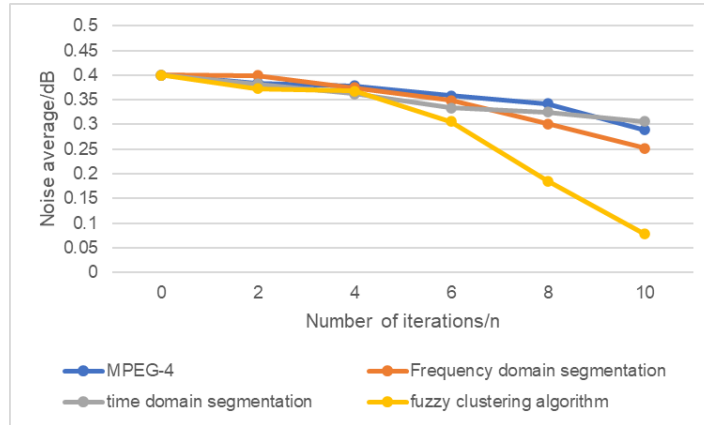
Fig. 4.2: The relationship between the number of iterations in paragraph 1 and the mean noise value.

4.2. Noise iteration performance. For the iterative ability of image segmentation algorithm against noise, the most fundamental requirement is that it can quickly achieve the purpose of self-adaptation. Figure 4.1 shows the average noise curve of two successively changing dynamic images in motion video recording. Fig. 4.2 and Fig. 4.3 shows the changes in the number of iterations for the average noise of various partitioning modes [16]. The overall increase in noise level off. After using this algorithm, the noise in the image is reduced to some extent [17]. The moving image segmentation algorithm based on fuzzy clustering is adopted. Repeat 6 times to reduce the noise of the image to 50%. The algorithm has good noise iteration.

4.3. Spatial distortion rate. Fig. 4.4 and 4.5 show the changes of spatial distortion rates of two dynamic images that change successively when they are processed by various division methods [18]. The spatial distortion rate is determined in the following manner:

$$s_n = \frac{\sum_{(u,v)} P^{ext}(u,v) \oplus P^{ref}(u,v)}{\sum_{(u,v)} P^{ext}(u,v)} \times 100\% \tag{4.2}$$

s_n represents the spatial distortion rate of the NTH frame; Where P^{ext}, P^{ref} represents the value of the divided pixel (u,v), and the value of the complete pixel [19]. The experimental results show that this method can effectively eliminate the| invalid pixels in the moving video, effectively suppress the noise in the moving
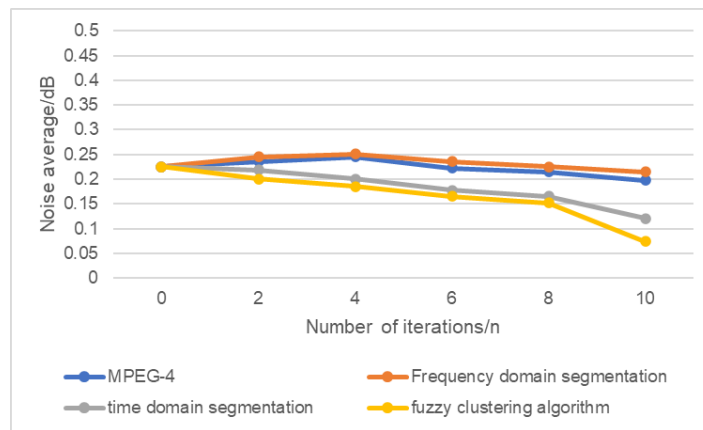
Fig. 4.3: Relation curve between the number of iterations in paragraph 2 and the mean noise value.
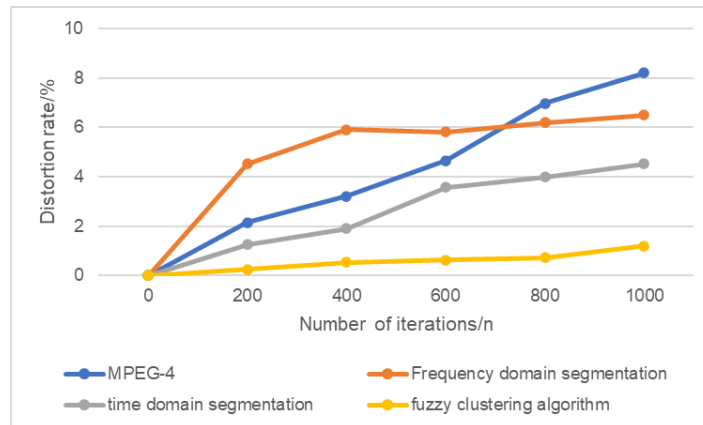
Fig. 4.4: Variation of the spatial distortion rate in paragraph 1.

video and obtain the obvious dynamic change law [20]. However, the other three kinds of algorithms have large spatial distortion, unstable change law, unable to effectively suppress noise points, and difficult to establish background. This leads to the segmentation of the image is not clear and other problems.

5. Conclusion. A moving image processing method based on fuzzy clustering is proposed. Compared with MPEG 4, frequency domain partition and time domain segmentation, the algorithm proposed in this project has higher application value in terms of spatial accuracy, noise iteration ability and spatial distortion rate. Physical education can promote national fitness and promote the development of competitive sports.

REFERENCES

[1] Rangasamy, K., As'ari, M. A., Rahmad, N. A., Ghazali, N. F., & Ismail, S. (2020). Deep learning in sport video analysis: a review. TELKOMNIKA (Telecommunication Computing Electronics and Control), 18(4), 1926-1933.
[2] Liu, Y., & Ji, Y. (2021). Target recognition of sport athletes based on deep learning and convolutional neural network. Journal of Intelligent & Fuzzy Systems, 40(2), 2253-2263.
[3] Zhao, Z., Liu, X., & She, X. (2021). Artificial intelligence based tracking model for functional sports training goals in competitive sports. Journal of Intelligent & Fuzzy Systems, 40(2), 3347-3359.
[4] Deng, Q., Zhang, Z., & Zhong, J. (2020). Image-free real-time 3-D tracking of a fast-moving object using dual-pixel detection. Optics Letters, 45(17), 4734-4737.
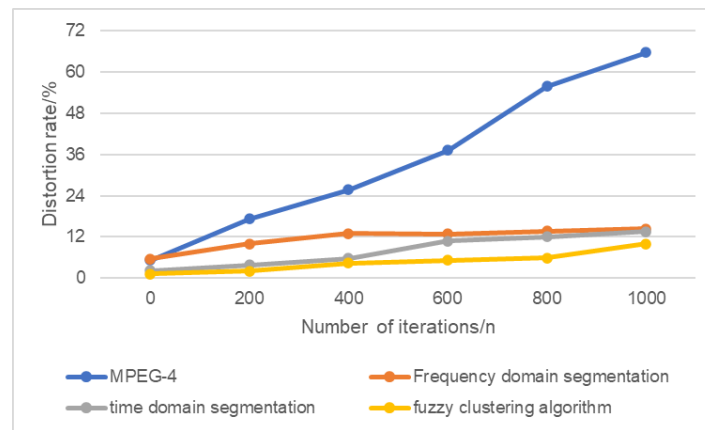
Fig. 4.5: Variation of spatial distortion rate in paragraph 2.

[5] Lu, Y., & An, S. (2020). Research on sports video detection technology motion 3D reconstruction based on hidden Markov model. Cluster Computing, 23(3), 1899-1909.

[6] Yan, L., Cengiz, K., & Sharma, A. (2021). An improved image processing algorithm for automatic defect inspection in TFT-LCD TCON. Nonlinear Engineering, 10(1), 293-303.

[7] Wu, S. (2021). Simulation of classroom student behavior recognition based on PSO-kNN algorithm and emotional image processing. Journal of Intelligent & Fuzzy Systems, 40(4), 7273-7283.

[8] Nakayama, Y., Lu, H., Li, Y., & Kamiya, T. (2020). WideSegNeXt: semantic image segmentation using wide residual network and NeXt dilated unit. IEEE Sensors Journal, 21(10), 11427-11434.

[9] Raabe, D., Nabben, R., & Memmert, D. (2023). Graph representations for the analysis of multi-agent spatiotemporal sports data. Applied Intelligence, 53(4), 3783-3803.

[10] Wang, T. (2022). Exploring intelligent image recognition technology of football robot using omnidirectional vision of internet of things. The Journal of Supercomputing, 78(8), 10501-10520.

[11] Zhou, G., Zhang, Z., Yin, W., Chen, H., Wang, L., Wang, D., & Ma, H. (2024). Surface defect detection of CFRP materials based on infrared thermography and Attention U-Net algorithm. Nondestructive Testing and Evaluation, 39(2), 238-257.

[12] Pasupa, K., Kittiworapanya, P., Hongngern, N., & Woraratpanya, K. (2022). Evaluation of deep learning algorithms for semantic segmentation of car parts. Complex & Intelligent Systems, 8(5), 3613-3625.

[13] Chen, C., Seo, H., Jun, C. H., & Zhao, Y. (2022). Pavement crack detection and classification based on fusion feature of LBP and PCA with SVM. International Journal of Pavement Engineering, 23(9), 3274-3283.

[14] Sun, Z., Xuan, P., Song, Z., Li, H., & Jia, R. (2022). A texture fused superpixel algorithm for coal mine waste rock image segmentation. International Journal of Coal Preparation and Utilization, 42(4), 1222-1233.

[15] Husain, A. A., Maity, T., & Yadav, R. K. (2020). Vehicle detection in intelligent transport system under a hazy environment: a survey. IET Image Processing, 14(1), 1-10.

[16] Liang, C. M., Li, Y. W., Liu, Y. H., Wen, P. F., & Yang, H. (2022). Segmentation and weight prediction of grape ear based on SFNet-ResNet18. Systems Science & Control Engineering, 10(1), 722-732.

[17] Wang, H., Minnema, J., Batenburg, K. J., Forouzanfar, T., Hu, F. J., & Wu, G. (2021). Multiclass CBCT image segmentation for orthodontics with deep learning. Journal of dental research, 100(9), 943-949.

[18] Wang, Y., Lv, H., Deng, R., & Zhuang, S. (2020). A comprehensive survey of optical remote sensing image segmentation methods. Canadian Journal of Remote Sensing, 46(5), 501-531.

[19] Cai, W., Song, Y., Duan, H., Xia, Z., & Wei, Z. (2022). Multi-feature fusion-guided multiscale bidirectional attention networks for logistics pallet segmentation. Computer Modeling in Engineering and Sciences, 131(3), 1539-1555.

[20] He, S., Wang, R., & Luo, H. (2022). Computing metasurfaces for all-optical image processing: a brief review. Nanophotonics, 11(6), 1083-1108.